14th IEA Heat Pump Conference
15-18 May 2023, Chicago, Illinois

Thermally driven industrial ionic liquid absorption heat pump dryer

Michael Schmid[a], Rohit Bhagwat[b], and Saeed Moghaddam[b*]

[a]Micro Nano Technologies, 747 SW 2nd Ave, Gainesville, FL, 32601, USA
[b]University of Florida, 939 Sweetwater Dr, MAE-A Bldg, RM 310, Gainesville, FL, 32611, USA
*Email: saeedmog@ufl.edu

Abstract

Drying, an energy-intensive process that is indispensable to many industries, accounts for 10–20% of the total industrial energy use in most developed countries. Thus, there are great incentives to reduce energy use in drying to lower its carbon footprint and improve process economics. However, challenging thermodynamic barriers have limited the opportunities to reduce energy consumption in the drying industry. The vapor compression system heat pump (VCSHP) has been established as a promising technology to improve the drying process efficiency. Fuel-flexible heat pump systems (operated by waste heat, solar-thermal, biomass, and green hydrogen) provide an off-grid alternative to VCSHP with attractive efficiency and economics. Here, two configurations of a thermally-driven ionic liquid semi-open absorption heat pump drying system are studied. Both systems utilize an adiabatic absorber to remove latent heat (moisture) from the process air and return its latent energy content as sensible heat to the process air (i.e., latent to sensible energy exchange takes place in the absorber). The systems' condenser heat is then recovered to further increase the process air temperature prior to its entry into the drying kiln. Test results show that our semi-open ionic liquid absorption heat pump approaches a moisture removal efficiency (MRE) of ~1.2 kg $H_2O/kWh_{primary}$ comparable with the VCSHP drying systems (available products have an average MRE 1.4 kg $H_2O/kWh_{primary}$). This level of performance, coupled with its fuel-flexibility, demonstrates the viability of the ionic liquid absorption heat pump technology in industrial drying.

Selection and/or peer-review under the responsibility of the organizers of the 14th IEA Heat Pump Conference 2023

Keywords: Absorption; Heat Pump; Drying;

1. Introduction

Drying is an indispensable technique for large-scale food preservation and lumber production. Dried foods offer numerous benefits including storage stability, ease of packaging, and reduction in transportation cost. Lumber is dried to enhance its stability and strength. However, drying is one of the most energy-intensive processes, accounting for 10–20% of the total industrial energy use in most developed countries [1]. The main reason for this is the high latent heat of evaporation of water and the relatively low energy efficiency of industrial dryers [2]. Thus, there are clear incentives to reduce energy use in drying to lower its carbon footprint and improve process economics. However, challenging thermodynamic barriers have limited the opportunities to reduce energy consumption.

Current vapor compression system heat pump (VCSHP) drying has been demonstrated as a state of the art, low energy drying technology applicable to the food and lumber industries [3]. VSCHP drying is a technology in which an air-to-air heat pump is used to dehumidify and heat air as the convective medium for drying of food and lumber materials [4]. Since the system is entirely re-circulatory, food and lumber products are dried in environmentally friendly conditions in an operation that is independent of outside ambient weather

* Corresponding author. *E-mail address:* saeedmog@ufl.edu

conditions. Energy consumption is significantly reduced with respect to other commonly used industrial drying technologies [5].

Recent work has demonstrated the dehumidification capability of a thermally driven semi-open absorption heat pump [6–9]. The semi-open absorption cycle operates at near ambient pressure, eliminating complexities and costs associated with conventional absorption cycles. An ionic liquid (IL) has been successfully implemented enabling the system operation at cycle conditions not possible with conventional salts and operation with inexpensive and passive controls. Herein, two configurations of the system are studied to establish their moisture removal efficiency (MRE). The performance of these two configurations is compared with VCSHP technology.

2. System

Single- (Figure 1a) and double-effect (Figure 1b) semi-open heat pump absorption cycles with heat recovery are studied at conditions representative of lumber drying kilns. These systems operate in a cycle in which water vapor is absorbed from the warm and humid air of the drying kiln. The water vapor is absorbed in the absorber and is subsequently liberated in the desorber(s) via heating. Within the absorber, the concentrated desiccant solution flows down the absorber plates while interfacing with the air flow through a porous membrane. The water vapor is absorbed by the solution. The dilute (i.e., water-rich) solution then exits the absorber and is pumped to the desorbers where it is regenerated. Depending on the configuration, one or two heat exchangers (SHXs) are used to recover heat of the solution exiting the desorber to elevate the temperature of the solution entering the desorber. In this application, the heat of the desorbed vapor/condensate is used to heat the process air. This enables the cycle to dehumidify and reheat the process air, prior to its reentry into the drying kiln.

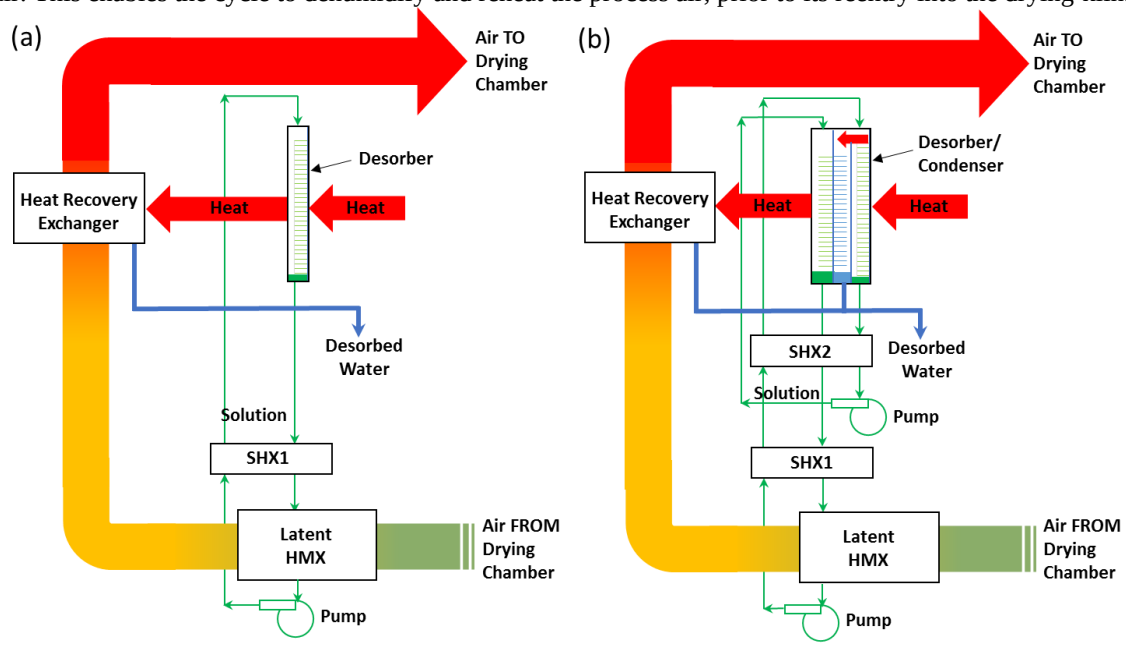

Figure. 1. The semi-open absorption single-effect (a) and double-effect (b) heat pump drying system configuration schematics.

2.1. Instrumentation Diagram

To validate performance of the single- and double-effect semi-open absorption cycles, and their associated moisture removal efficiencies, two systems were studied. Each experimental test setup consisted of two primary flow loops including the solution and air flow loops as well as three secondary flow loops; the heating oil loop, the condenser/absorber cooling water loop, and the air-cooling loop (Figure 2). The IL solution exiting the absorber is pumped to the desorber by a small variable speed gear pump. The absorber is located within the closed air loop (cf. Figure 2). In the single-effect configuration (Figure 2a), the solution exiting the desorber returns to the absorber to complete the solution flow loop. In the double-effect configuration, the solution exiting the upper desorber is pumped to the lower desorber by a second variable speed gear pump. The solution exiting the lower desorber returns to the absorber to complete the solution flow loop. To control the humidity level within the air loop, a steam generator in conjunction with a custom-made steam distribution manifold are utilized. To control the air temperature, a secondary water loop is connected to a heating/cooling coil installed

within the air duct. A variable speed axial fan is used to circulate air through the air loop. The heating oil loop, which powers the upper desorber, utilizes a heating oil bath and synthetic oil SIL 180. As the test setups only validated the cycle performance, they did not contain a heat recovery exchanger (Figure 1) to sensibly heat the air prior to its exit back into the drying kiln. As such, a water chiller is used to maintain the lower condenser at the desired temperature.

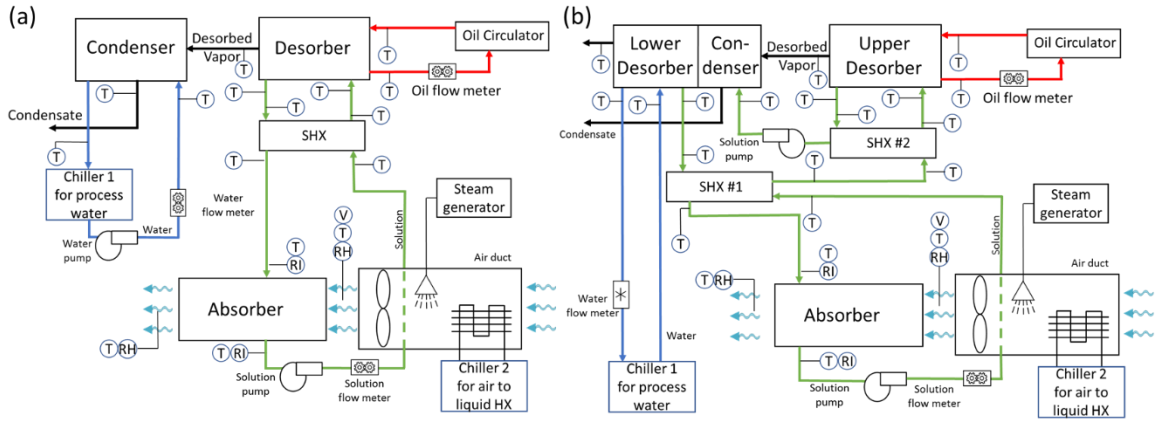

Figure. 2. Instrumentation diagram of the single-effect (a) and double-effect (b) experimental test systems.

The solution and water flow rates are measured using positive displacement and turbine flow meters, respectively. Due to the elevated temperature of the oil flow loop, a high-temperature positive displacement flow meter is used to measure the oil flow rate. The air flow rate is measured using a pitot tube sensing element mounted within the air loop duct. Multiple sensing ports along the length of the sensing element are used, and internally averaged to ensure accurate air flow rate measurement. All liquid temperatures were measured using T-type thermocouples. The process air temperature and relative humidity are measured using thin-film capacitive sensors. The absorber solution inlet and outlet concentrations are measured using two inline refractive index (RI) sensors. RI instead of Coriolis effect is used because the variation in density for ILs is insignificant over a wide concentration range, making accurate measurement of the concentration infeasible. Curve fits have been developed to establish RI values as a function of IL concentration and temperature. The primary system temperature, flow rate, RI, and air velocity are recorded using a data acquisition system. A second data acquisition system is used to record the air temperature and relative humidity. Time stamps are used to combine the data collected by each data acquisition system to enable a cycle level data analysis.

2.2. Absorber

In the HP drying application, humid warm air is removed, dehumidified, heated, and returned to the drying kiln. To support this process, an adiabatic absorber fabricated from Acrylonitrile Butadiene Styrene (ABS) sheets is used. The desiccant solution flows on the two surfaces of each absorber plate. The plate surfaces are machined to include features designed to slow and spread the solution flow to “wet” the entire surface (front and back) of each sheet [10,11]. A membrane is then bonded over the surface features to constrain the solution. Lastly, manifolds are bonded on the top and bottom of each side of the ABS sheet-membrane assembly (i.e., a panel) to direct the IL flow through the gap formed in between the ABS surface and membrane. Air flows across the panels (cf. Figure 3) through 3 mm gaps formed in between them within the absorber assembly. To support our modelling efforts, an absorber was fabricated and tested. Geometrical characteristics of the absorber are provided in Table 1. The test data was used to validate the absorber model [12].

Table 1: Absorber design properties and parameters.

Parameter	Value
Number of panels	14
Active Surface area (m^2)	3.30
Active plate Volume (m^3)	0.0091
Active surface area/volume ratio (m^{-1})	363.6

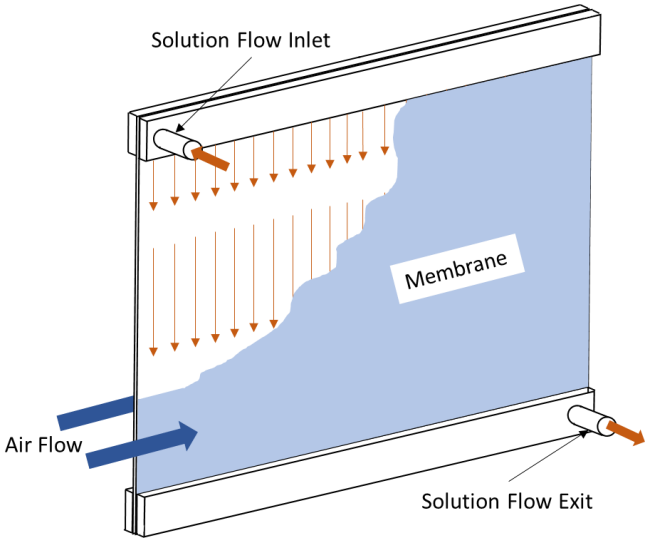

Figure 3. A schematic of a single absorber plate showing that air flows across the membrane while exchanging moisture with the desiccant solution constrained behind the membrane.

2.3. Desorbers and Condensers

In the double-effect configuration, the desorber/condenser module contains upper and lower desorbers and condensers (Figure 4a). In this configuration, heat is added to the dilute solution in the upper desorber using silicone oil in a counter flow heat exchange configuration. The desorbed vapor is then condensed in the upper condenser. The heat released from the vapor is used to heat the solution in the lower desorber. The solution leaving the upper desorber is cycled back to the low desorber after it passes through a heat recovery heat exchanger (Figure 1). The vapor desorbed in the lower desorber is condensed in the lower condenser. In the single-effect configuration (Figure 2a), heat is only used once in the desorption process. Thus, only a single desorber and condenser are contained in the module. The heat from the lower condenser (double-effect) and the condenser (single-effect) are used in a steam/air heat exchanger to heat the process air. A single- and a double-effect desorbers/condensers module (Figure 4b) were fabricated and have been used to test the performance of the single and double-effect test systems.

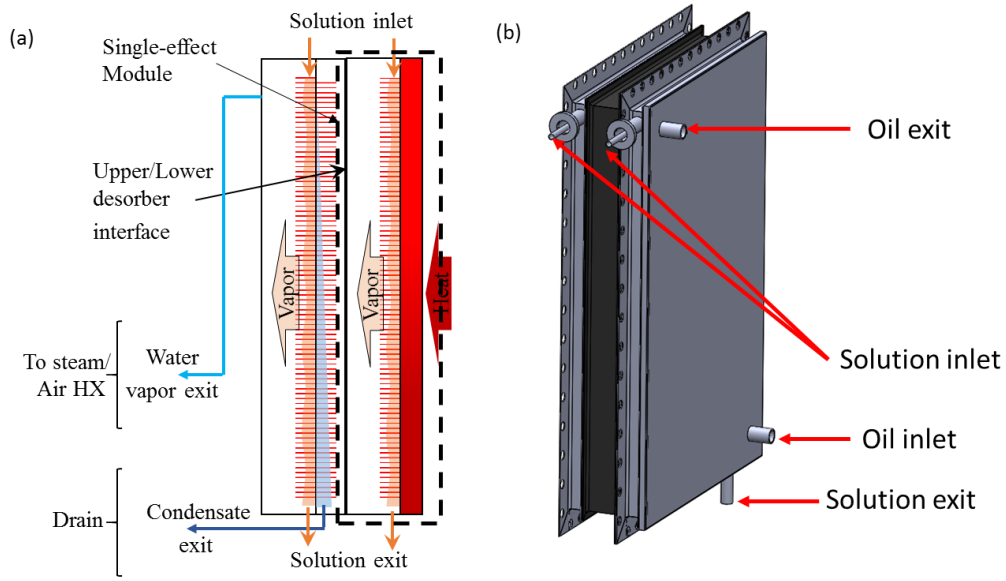

Figure 4. The absorption cycle desorber/condenser assembly schematic (a) and assembly 3-D model (b).

2.4. Ionic Liquids

ILs are broadly defined as low temperature molten salts composed of large asymmetric organic cations and inorganic or organic anions that are moisture and air stable at room temperature [13], [14]. ILs exhibit properties required for absorption dehumidification systems including thermal stability, negligible vapor pressure, high solubility in water, and low corrosion towards metals, making their use promising in absorption systems [15]. In liquid desiccant absorption systems, the dehumidification capability of the desiccant is considered its most critical thermo-physical property. This characteristic of the desiccant is best represented by its water vapor pressure at a given concentration and temperature.

Another key factor that dictates the dehumidification system design and whether an IL-based system can be successfully built is the IL viscosity. Our studies [9], [7], [16], have shown that the IL viscosity impacts the design of middle and low temperature components of the system the most, consisting of the absorber and solution heat exchanger. The high operating temperature of our desorber greatly reduces the IL solution viscosity such it is not the prominent factor in design considerations. Viscosity is a key constrain in design of the solution heat exchanger when the IL flow from the desorber to absorber is driven by gravity. Furthermore, design of the IL flow distribution within the absorber is impacted by the IL viscosity. Hence, assessing utility of one IL versus another involves comparing their viscosity..Table 2 compares viscosity of the IL used in this study and LiBr, LiCl, and [EMIM]OAc. While viscosity of both ILs is similar, it is 2-3 times higher than that of the LiBr and LiCl.

Table 2. Dynamic viscosity comparison for different liquid desiccants.

Desiccant	Viscosity (Pa-s)	Stability Limit (°C)
LiCl (20 °C, 40%)	0.0096	NA
LiBr (20°C, 53%)	0.0051	NA
[EMIM]OAc (20°C, 73%)	0.0233	~100

2.5. Data reduction and uncertainty analysis

The system performance presented in the results and discussion section is calculated based on the measured data described above. The system latent capacity is calculated using Eq. (1).

$$Q_{latent} = \dot{V}_{air}\, \rho_{air}\, h_{fg}\, (\omega_{air\_in} - \omega_{air\_out}) \tag{1}$$

where $\dot{V}_{air}$ is the absorber air flow rate; ω_{air_in} and ω_{air_out} are the absorber air inlet and exit absolute humidity, respectively; ρ_{air} is the air density as calculated from standard tables using the measured air inlet conditions; and h_{fg} is the water latent heat of evaporation. The desorber heat input is calculated using Eq. (2).

$$Q_{oil} = \dot{V}_{oil}\, \rho_{oil}\, c_{p\_oil} (T_{des\_oil\_in} - T_{des\_oil\_out}) \tag{2}$$

where $\dot{V}_{oil}$ is the desorber oil flow rate; $T_{des\_oil\_in}$ and $T_{des\_oil\_out}$ are the desorber oil inlet and outlet temperatures, respectively; ρ_{oil} is the oil density; and c_{p_oil} is the oil thermal capacity calculated using curve fits derived from data provided by Clearco for their SIL 180 silicone oil. The system latent heat capacity along with the desorber heat input are used in Eq. (3) to calculate the system dehumidification COP.

$$COP_{dehumidification} = \frac{Q_{latent}}{Q_{oil}} \tag{3}$$

The moisture removal efficiency (MRE) was estimated using Eq. (4).

$$MRE = \frac{\dot{V}_{air}\, \rho_{air}\, (\omega_{air\_in} - \omega_{air\_out})}{Q_{oil}} \tag{4}$$

The uncertainty was calculated using an engineering equation solver (EES) uncertainty propagation subroutine. The subroutine is based on NIST guidelines[17] and assuming that the individual measurements are uncorrelated and random, the uncertainty in the calculated quantity can be estimated using Eq. (5).

$$U_Y = \sqrt{\sum_i \left[\frac{\partial Y}{\partial X}\right]^2 U_{X_i}^2} \tag{5}$$

Table 2 below lists all the relevant measurement errors and uncertainties in this experimental study.

Table 2. Measurement error and uncertainty propagation.

Variable	Uncertainty
Fluid temperatures -All T-type TC	±0.8°C
Solution volumetric flow rate	±0.25% reading
Solution RI	±0.5% scale range (0.0003nD)
Water volumetric flow rate	±1% full scale (0.5 LPM)
Air volumetric flow rate	±2% reading
Oil volumetric flow rate	±0.5% reading
Air temperature	±0.3°C
Air relative humidity	±1.8% RH
Oil heat	±3.7%
Water heat	±2.0%
Concentration (X%)	±0.15%
COP	±4.2%

3. Results and discussions

The experimental test loop was run to validate the dehumidification performance of the two different configurations of the semi-open absorption cycle as a heat pump dryer. The absorber implemented for this test was approximately 35×35×8 cm (H×W×D) in size with 3.3m^2 of active surface area (Table 1). It is noted that the absorber and desorber architectures are modular, enabling the increase in capacity through the addition of plates, without loss in efficiency. In typical drying applications, it is desirable to dehumidify the process air and elevate its temperature within the absorber. As shown in Figure 5, the system latent capacity is a function of the inlet air dewpoint temperature because the air moisture increases with increasing the dewpoint temperature. Within the absorber, the primary difference between the single- and double-effect system configurations is the inlet solution concentration and temperature. In this study, across the spectrum of single-effect experimental data, the absorber solution inlet concentration was kept constant at ~88%. The absorber inlet solution concentration in the double-effect experimental is maintained constant at ~92%. As the water absorption process is driven by the difference in vapor pressure between the process air and the desiccant solution (solution vapor pressure decreases with increasing concentration), the latent capacity of the double-effect system at these same conditions (Figure 5) is expected to be greater.

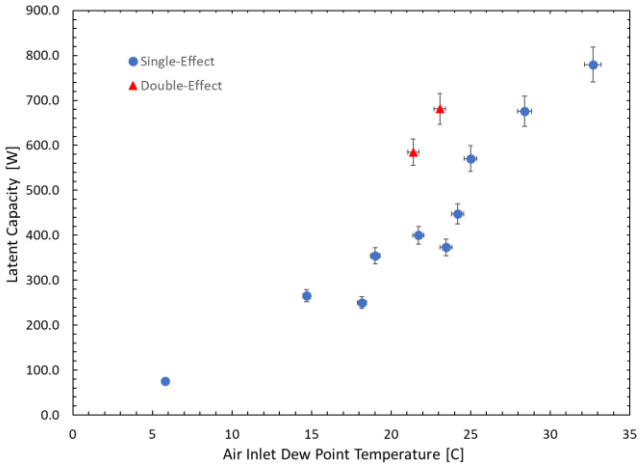

Figure. 5. Single- and double- effect system latent capacity as a function of inlet air dewpoint temperatures. The inlet air, IL solution, and oil flow rates as well as the oil inlet temperatures have been held constant at 155 cfm, 300 mlpm, 2.85 lpm, and 148 °C, respectively. The solution flow rate for the two double-effect data points is 125 mlpm.

In the drying application it is also beneficial to raise the temperature of the process air at the absorber exit. This limits the amount of condenser heat recovery required to achieve the desired exit air temperature conditions. The amount of sensible heat transferred to the process air is a function of the absorber inlet air dry bulb temperature and the inlet solution temperature. As shown in Figure 6, as the difference between the solution and air inlet temperatures increases (the solution is hotter than the inlet air) the process air dry bulb temperature rises. At large solution/air inlet temperature differences, the process air is heated up to ~6 °C. It is

noted that although the same solution and air inlet temperature difference can be observed at different operating conditions, leading to a range of absorber air temperature increases, there is a general trend of increasing absorber with increasing solution/air inlet temperature difference. The low air temperature rise in the double-effect system is attributable to the low solution flow rate (125 mlpm). At this low flow rate, the heat transfer resistance between the solution and the air flows increases due to an increased air gap between the membrane and the solution.

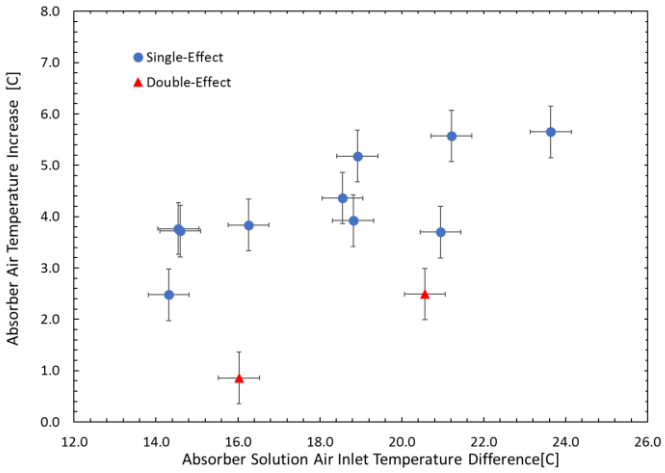

Figure 6. 1. Process air dry bulb temperature increase, as a function of the single- and double-effect absorber inlet solution/air temperature difference. The inlet air, IL solution, and oil flow rates as well as the oil inlet temperature have been held constant at 155 cfm, 300 mlpm, 2.85 lpm, and 148 °C, respectively. The solution flow rate for the two double-effect data points is 125 mlpm.

The MRE of the single- and double-effect systems as calculated on a primary energy basis is shown in Figure 7. To convert the MRE as calculated by Eq. 4, a burner efficiency of 0.85 and a site-to-source ratio of 1.05 (natural gas) has been used to adjust the amount of energy (Q_{oil}) required to drive the system. As this system can use solar thermal, biomass, waste heat, etc., it is believed that this burner efficiency/natural gas site-to-source ratio provides a representative estimate of the system's primary energy consumption. As can be seen in Figure 7, the single-effect primary MRE approaches 1.25 kg/kWh$_{primary}$ with increasing inlet air dewpoint. At the same conditions, the estimated theoretical performance of the double-effect system (Figure 7) approaches an MRE of 2.35 kg/kWh$_{primary.}$ As the testing has just begun, the MRE performance of the double-effect system at a low solution flow rate of 125 mplm is presented in Figure 7. As the double-effect testing continues over the coming month, a complete set of data at a solution flow rate of 300 mlpm will be incorporated in this figure.

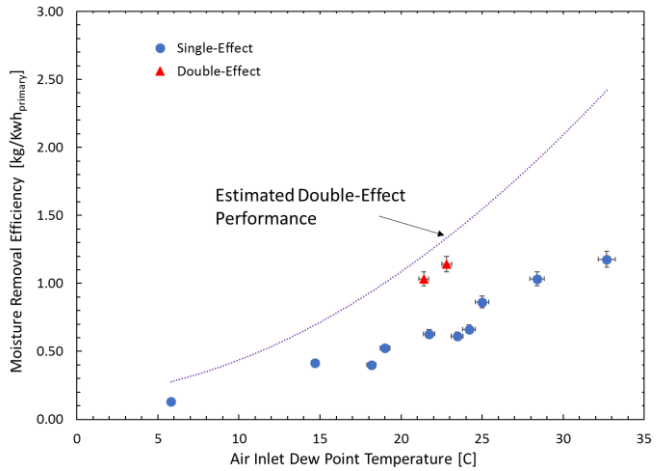

Figure 7. Single- and double-effect system primary moisture removal efficiency as a function of the air inlet dew point temperature. The inlet air, IL solution, and oil flow rates as well as the oil and inlet temperature have been held constant at 155 cfm, 300 mlpm, 2.85 lpm, and 148 °C respectively for the single effect system. The solution flow rate for the two double-effect data points is 125 mlpm.

This preliminary MRE data compares well to the performance of current VCSHP systems (0.65-1.53 $Kg/kWh_{primary}$) [18–20] (Figure 8) when the data is converted from site to primary energy using a primary energy factor of 2.8. Improvements in the system's MRE performance are expected with the optimization of the solution and air flow rates as well as system components.

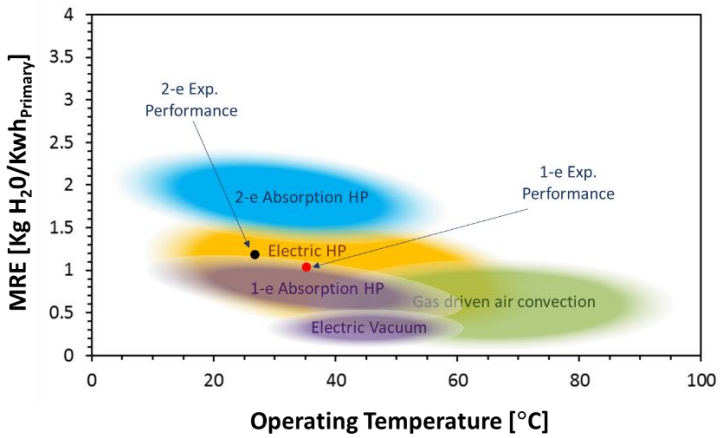

Figure 8. A comparison of drying technologies primary energy MRE as a function of system operating temperature.

4. Conclusions

Laboratory-scale IL single- and double-effect absorption heat pump drying systems were experimentally tested across a range of inlet air conditions representative of those found in low temperature drying applications. The single-effect system demonstrated a MRE of 1.2 $kg/kWh_{primary}$. The MRE performance of the double-effect system is projected to reach 2.35 $kg/kWh_{primary}$. This preliminary performance compares well with the current state-of-the-art VCSHP performance based on the primary energy consumption. The use of IL demonstrated the robustness of the system without control equipment for mitigating crystallization. Further optimization of the system operating conditions and components are ongoing. This thermally-driven technology could facilitate implementation of waste heat, solar thermal, biomass, and green hydrogen powered industrial drying systems.

Nomenclature

ABS	acrylonitrile butadiene styrene
CFM	cubic feet per minute
COP	coefficient of performance
$COP_{dehumidification}$	dehumidification capacity (latent cooling)/thermal energy consumed
HP	heat pump
HX	heat exchanger
IL	ionic liquid
LPM	liters per minute
mLPM	milliliters per minute
PTFE	polytetrafluoroethylene
RI	refractive index
RH	relative humidity
SHX	solution heat exchanger
$\dot{m}$	mass flow rate (kg/sec)
MRE	moisture removal efficiency
T	temperature (°C)
VCSHP	vapor compression system heat pump

Acknowledgements

This work was sponsored by the U. S. Department of Energy, Advanced Research Projects Agency (Arpa-e), under Award Number DE-AR0001488 with Micro Nano Technologies. The authors would also like to acknowledge Mr. Pieter De Bock from Arpa-e for his support of this research.

References

[1] Kemp IC. Fundamentals of Energy Analysis of Dryers. Modern Drying Technology, John Wiley & Sons, Ltd; 2014, p. 1–45. https://doi.org/https://doi.org/10.1002/9783527631728.ch21.

[2] Brunetti L, Giametta F, Catalano P, Villani F, Fioralba J, Fucci F, et al. Energy consumption and analysis of industrial drying plants for fresh pasta process. Journal of Agricultural Engineering 2015;46:167–71. https://doi.org/10.4081/jae.2015.478.

[3] Menon A, Stojceska V, Tassou SA. A systematic review on the recent advances of the energy efficiency improvements in non-conventional food drying technologies. Trends Food Sci Technol 2020;100:67–76. https://doi.org/10.1016/j.tifs.2020.03.014.

[4] Perera CO, Rahman MS. Heat pump dehumidifier drying of food. Trends Food Sci Technol 1997;8:75–9. https://doi.org/10.1016/S0924-2244(97)01013-3.

[5] Fayose F, Huan Z. Heat pump drying of fruits and vegetables: Principles and potentials for Sub-Saharan Africa. Int J Food Sci 2016;2016. https://doi.org/10.1155/2016/9673029.

[6] Chugh D, Gluesenkamp K, Abdelaziz O, Moghaddam S. Ionic liquid-based hybrid absorption cycle for water heating, dehumidification, and cooling. Appl Energy 2017;202:746–54. https://doi.org/10.1016/j.apenergy.2017.05.161.

[7] Chugh D, Gluesenkamp KR, Abu-Heiba A, Alipanah M, Fazeli A, Rode R, et al. Experimental evaluation of a semi-open membrane-based absorption heat pump system utilizing ionic liquids. Appl Energy 2019;239:919–27. https://doi.org/10.1016/j.apenergy.2019.01.251.

[8] Gluesenkamp KR, Kumar N, Abu-heiba A, Patel V. Semi-open absorption water heater : experimental results 2020:1–11.

[9] Gluesenkamp KR, Chugh D, Abdelaziz O, Moghaddam S. Efficiency analysis of semi-open sorption heat pump systems. Renew Energy 2016:1–10. https://doi.org/10.1016/j.renene.2016.07.075.

[10] Mortazavi M, Isfahani Nasr R, Bigham S, Moghaddam S. Absorption characteristics of falling film LiBr (lithium bromide) solution over a finned structure. Energy 2015;87:270–8.

[11] Nasr Isfahani R, Bigham S, Mortazavi M, Wei X, Moghaddam S. Impact of micromixing on performance of a membrane-based absorber. Energy 2015. https://doi.org/10.1016/j.energy.2015.08.006.

[12] Bhagwat R, Schmid M, Moghaddam S. Experimental and numerical analysis of a three-fluid membrane-based ionic liquid desiccant absorber. Int J Heat Mass Transf 2022;183:122122. https://doi.org/10.1016/j.ijheatmasstransfer.2021.122122.

[13] Shah FU, An R, Muhammad N. Editorial: Properties and Applications of Ionic Liquids in Energy and Environmental Science. Front Chem 2020;8:1–3. https://doi.org/10.3389/fchem.2020.627213.

[14] Kim YJ, Kim S, Joshi YK, Fedorov AG, Kohl PA. Thermodynamic analysis of an absorption refrigeration system with ionic-liquid/refrigerant mixture as a working fluid. Energy 2012;44:1005–16. https://doi.org/10.1016/j.energy.2012.04.048.

[15] Qu M, Abdelaziz O, Sun XG, Yin H. Aqueous solution of [EMIM][OAc]: Property formulations for use in air conditioning equipment design. Appl Therm Eng 2017;124:271–8. https://doi.org/10.1016/j.applthermaleng.2017.05.167.

[16] Chugh D, Gluesenkamp K, Abdelaziz O, Moghaddam S. Ionic liquid-based hybrid absorption cycle for water heating, dehumidification, and cooling. Appl Energy 2017;202. https://doi.org/10.1016/j.apenergy.2017.05.161.

[17] Taylor BN, Kuyatt CE. Guidelines for Evaluating and Expressing the Uncertainty of NIST Measurement Results. Technology (Singap World Sci) 1994:2.

[18] Closas AA, Villanueva EP. Determination of Specific Moisture Evaporation Rate, Energy Consumption and Specific Energy Consumption at Varying Sample Load Capacity per Batch Drying in a Heat Pump Dryer. International Journal of Engineering and Techniques 2017;3.

[19] Yang KS, Hamid K, Wu SK, Sajjad U, Wang CC. Experimental analysis of a heat pump dryer with an external desiccant wheel dryer. Processes 2021;9. https://doi.org/10.3390/pr9071216.

[20] Stawreberg L, Nilsson L. Modelling of Specific Moisture Extraction Rate and Leakage Ratio in a Condensing Tumble Dryer. Appl Therm Eng 2010;30:2173–9. https://doi.org/10.1016/j.applthermaleng.2010.05.030.